Characterizing Hydrogen Bonds in Intact RNA from MS2 Bacteriophage Using Solid State Magic Angle Spinning NMR

Orr Simon Lusky[1], Moran Meir [2], A. Goldbourt[1*]

[1]*School of Chemistry, Faculty of Exact sciences, and* [2]*School of Molecular Cell Biology and Biotechnology, The George S. Wise Faculty of Life Sciences, Tel Aviv University, Tel Aviv, Israel.*

[*]amirgo@tauex.tau.ac.il

Abstract

Ribonucleic acid (RNA) is a polymer with pivotal functions in many biological processes. RNA structure determination is thus a vital step towards understanding its function. The secondary structure of RNA is stabilized by hydrogen bonds formed between nucleotide base pairs and it defines the positions and shapes of functional stem-loops, internal loops, bulges, and other functional and structural elements. In this work we present a methodology for studying large intact RNA molecules using homonuclear ^{15}N solid state nuclear magnetic resonance (NMR) spectroscopy. We show that Proton Driven Spin Diffusion (PDSD) experiments with long mixing times, up to 16s, improved by the incorporation of ^{1}H Radiofrequency Dipolar Recoupling (RFDR) pulses, reveal key hydrogen-bond contacts. In the full-length RNA isolated from MS2 phage, we observed strong and dominant contributions of G-C Watson-Crick base pairs, and beyond these common interactions, we observe a significant contribution of the G-U wobble base pairs. Using the improved technique facilitates characterization of hydrogen-bond types in intact large-scale RNA using solid-state NMR. It can be highly useful to guide secondary structure prediction techniques, and possibly to refine higher resolution structure determination methods.

Introduction

RNA structure has long been a subject of intensive studies, mainly in view of the discovery that RNA is not only a delivery vehicle (mRNA) that transfers the DNA genetic code to the ribosome. Non-coding RNA molecules adopt a large variety of three-dimensional structures serving many cellular roles (1, 2). tRNA delivers amino acids to the ribosome that also contains ribosomal RNAs as part of its structure. Riboswitches regulate gene expression, ribozymes can catalyse various reactions similarly to enzymes, and additional roles of RNA exist and continue to be discovered, the most recent one being of RNA-glycan conjugates displayed on the cell surface (3).

Generally, most structural studies are performed on small synthetic RNA molecules. For example, structures solved by NMR (4, 5) and X-ray crystallography (6) reveal various secondary structure elements such as base-paired helices, stem-loops, bulges and more. Structures of protein-RNA complexes are also prevalent, and were determined using various techniques such as cryogenic electron microscopy (CryoEM) (7), X-ray (8) and solution NMR (9). Solid state NMR has also provided structures of isolated RNA molecules or in complex with proteins (10, 11).

Large RNA molecules (>100nt) are challenging for solution NMR due to high spectral overlap and for larger sizes, due to decreased relaxation times. Such limitations are partially solved by segmentally labelling the RNA to reduce the spectral congestion (12, 13). They are also hard to obtain by crystallography techniques, and thus advanced sequence-based algorithms are used to predict their secondary structure. Such techniques are based on minimizing the free energy on the basis of the hydrogen bond patterns (14, 15). Other methods for assessing the structure of large RNA molecules utilize enzymatic digestion, radical labelling and more (16).

The base pairs in polynucleic acids are stabilized by the hydrogen bonds. Canonical base pairs are formed between the nucleotides adenine (A) and uracil (U), and cytosine (C) and guanine (G). The canonical and most common Watson-Crick (WC) base-pairs are formed between the nucleus bases, and in RNA are referred to as the 'Watson-Crick edge' (17). This type of bond is illustrated in figure 1a. However, there are other possible geometries for hydrogen bonds to form, namely the sugar edge and the Hoogsteen edge, as illustrated in figure 1b. Two nucleotides can form hydrogen bonds involving each pair of the three edges. Together with cis and trans orientations of the glycoside bond, there can be twelve types of hydrogen bonds giving the RNA flexibility in tertiary structure formation. Therefore, detection of the interacting edge of the hydrogen bond is essential to understanding RNA structure.

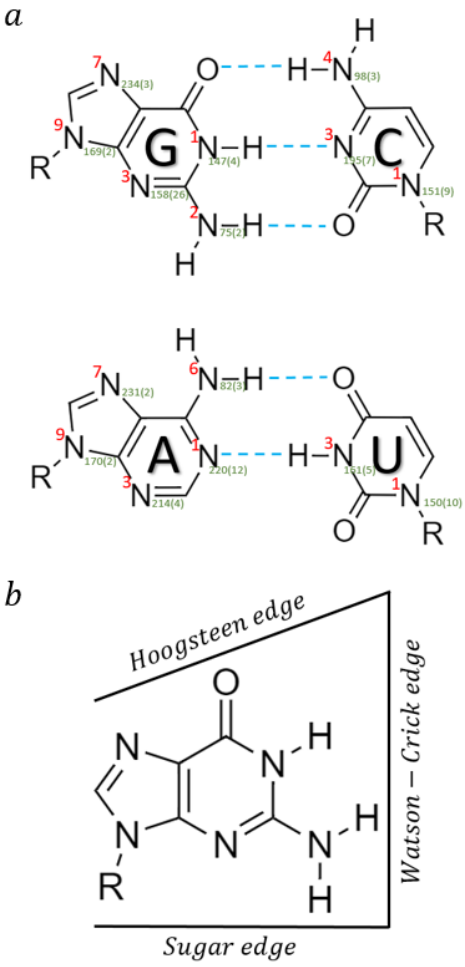

Figure 1: (a) Scheme of canonical Watson-Crick hydrogen bonds between nucleotides. The dashed blue lines represent the hydrogen bond. Red numbers represent the nitrogen BMRB nomenclature. Green numbers represent the average ^{15}N chemical shifts in ppm of the nucleus, and standard deviation in brackets. R stands for ribose ring. (b) A guanine nitrogenous base with its three edges types.

Hydrogen bonds can be distinguished and characterized by NMR and in large RNA molecules, by solid-state NMR. One of the key advantages of Solid-state NMR is the ability to study non-crystalline systems and the property that linewidth do not depend on molecular weight. The method has been successfully used to study various types of biological systems including folded and unfolded proteins, protein-DNA complexes, protein-RNA complexes, intact viruses and more (18–20). Recent efforts into studies of RNA has recently been reviewed by Marchanka (21) and by Wang (22). Those mainly include synthetic RNA molecules with or without bound proteins. For example, a 23-mer RNA fragment of HIV RNA and a $(CUG)_{97}$ RNA molecule were studied using ^{15}N-^{15}N correlations (23, 24) and

^{1}H-detected ^{15}N correlations at fast MAS (25). However, intact non-repetitive long RNA leads to high spectral congestion, which does not allow a resonance assignment for each nucleotide separately. Yet, it does hold information on the native hydrogen bonding patterns.

RNA viruses are common in nature. The size of RNA can be a few thousands of bases as in small spherical bacteriophages (26), or as large as 30 thousand bases, as in the case of SARS-CoV-2 (27). RNA viruses are fast mutating and therefore pose constant risk for global pandemics (28), as encountered in this past year. The packing, folding, and capsid binding properties of RNA within the context of intact viruses is therefore important to understand and we constantly seek methods aimed to study intact viruses or isolated intact RNA.

MS2 bacteriophage infects *Escherichia Coli* (E. Coli) bacteria bearing positive F pili. It contains a 3,569 nucleotide-long single stranded RNA, encapsulated in a capsid made of 89 copies of coat protein dimers, and a maturation protein. Despite being the first RNA molecule to be sequenced (29), initially structural studies focused on interactions of the capsid protein with small RNA epitopes (30–32). Only recently the interaction of the full-length RNA with the MS2 capsid in a wild-type viral particle was studied in detail using CryoEM. Initially a resolution of 8.7Å (33) was obtained revealing a network of stem loop regions in the RNA. Later on, the resolution was significantly improved to 3.6Å for the capsid and 6Å for the RNA(34). This resolution was sufficient for tracing the secondary structure motifs of different segments in the RNA revealing unprecedented details on its structure. In particular, the identity of the bases involved in base-pair interactions could be determined for approximately two-thirds of the sequence.

Here we show how ^{15}N correlations in solid-state NMR can be used to study the intact isolated RNA extracted from the MS2 phage. By improving ^{15}N-^{15}N proton-driven spin-diffusion polarization transfer (35) with radio-frequency driven recoupling (36) applied to the ^{1}H channel, which we term PDSD-RFDR, we show how hydrogen-bonds can be detected and characterized. From the type of nitrogen atoms involved, we can also estimate the type and face of those hydrogen bonds. We then compare the patterns we observe in the isolated RNA to that of the enclosed RNA derived from cryoEM.

Materials and Methods

Sample preparation. Wild type MS2 bacteriophage was produced by infecting cultures of *Escherichia Coli* strain C3000 and purified using our lab protocols for phage preparation (37). The RNA was harvested from the phage using a method similar to the one described by Meir et. al. (38). Phage were vortexed in TRIzol (TriReagent®), resuspended in isopropanol, followed by cold ethanol precipitation. The total yield of RNA from one litter bacterial culture was on average ~24 mg. The RNA precipitate was packed into a 4mm ZrO_2 MAS rotor using a centrifuge and then used for NMR experiments. More details on MS2 phage preparation and purifications as well as RNA isolation appear in the supporting information (SI).

NMR methods. All experiments were carried out on Bruker Avance III NMR spectrometer operating at 9.4T and equipped with a MAS 4mm probe. Two-dimensional ^{15}N-^{15}N

correlation experiment were collected using PDSD (35) experiments with mixing times up to 16s. Additional PDSD experiments were acquired by adding rotor-synchronized π pulses (as in radio-frequency driven recoupling, RFDR (36)) to the ^{1}H channel during the mixing time (2s, 8s). We term this experiment PDSD-RFDR. A complete list of experimental parameters appears in the supporting information Table S1. All experiments were performed using a spinning speed of 8 kHz and a set temperature of -28°C. The chemical shifts of ^{15}N were referenced using $^{15}NH_4Cl$ (39.3ppm (39))

Data Analysis. NMR data were processed using TopSpin3.5 and NMRPipe (40). Analysis was performed using SPARKY version 3.134 (41).

Numerical Simulation. The NMR simulation package SIMPSON (42) was used to verify the physical basis for the enhancement by RFDR. A SIMPSON script was written to show that the application of π pulses on protons enhances the magnetization transfer between two X spins in a X_2H_3 spin system. The script, the dipolar couplings used, and the magnetization build-up curves appear in the supporting information.

Results and Discussion

Identification of ^{15}N resonances. A typical two-dimensional ^{15}N-^{15}N proton-driven spin-diffusion (PDSD) solid-state MAS NMR correlation spectrum of MS2-RNA is shown in figure 2a. The off-diagonal correlation signals result from the dipolar coupling between ^{15}N nuclei that are proximate in space, probably not beyond ~4 Å. In order to obtain them with sufficient sensitivity it was necessary to significantly increase the mixing time up to 16 sec (exploiting the long T_1 of the ^{15}N spins) and simultaneously reduce the spinning speed to 8 kHz (thus reducing MAS averaging of the dipolar interaction). Similar to our previous study on intact T7 bacteriophage dsDNA (43), also here we see clear asymmetry in the spectrum resulting from the excitation difference between primary, secondary, and tertiary amines, and between nucleobases having more or less hydrogen atoms.

The resonances can be assigned to one of the four nucleotides (Fig. 1a) but not to a specific nucleotide in the sequence (totalling 3569 bases). The assignment process relied on data from the biological magnetic resonance bank (BMRB) for RNA and on the correlations observed in the spectrum as follows. Figure 2b shows blocks centred at positions corresponding to correlations between average RNA shifts of individual nucleotides (differentiated by colour). Their size is given by the standard deviation of the shifts according to the BMRB. The average chemical shifts (and their standard deviations) are explicitly given in figure 1a. Peaks from spectra similar to that in figure 2a were then marked on the predicted positions and assigned to the corresponding nucleotides. Many of the signals are easily identified. For example, primary amines are unique having shifts of 82 ppm (Adenosine N6, or in short A6), 75 ppm (Guanosine N2, G2), and 98 ppm (Cytidine N4, C4). Additional unique individual shifts are C3 (195 ppm), A3 (215 ppm) and A1(220 ppm) with the latter having a rather large standard deviation (11 ppm). Other shifts have to be determined from two or three options (G1, U1, C1 at ~150 ppm; U3, G3 at ~160 ppm; G9, A9 at ~170 ppm; A7, G7 at ~231 ppm), with uracil being the most difficult to identify unambiguously. Yet, correlations to resolved signals and "sidechain walks" (44) along proximate nitrogen nuclei in the same base are sufficient to identify the different

nucleotides. In the spectrum shown in Figure 2a, the different ^{15}N signals of the G-base are coloured and the linkage G2-G1-G9-G3-G7 can be clearly identified. Similarly, other bases are assigned. The full assignment table appears in Table 1, summing up to 13 out of 15 ^{15}N signals.

Table 1: ^{15}N chemical shifts (in ppm) of MS2-RNA. Unassigned nuclei are indicated by grey cells. Dashes indicate non-existing atoms.

	N1	N2	N3	N4	N6	N7	N9
A	222.0	-	213.2	-	83.8	231.2	
C	151.4	-	196.8	99.0	-	-	-
G	147.5	75.1	162.7	-	-	234.4	170.3
U		-	159.1	-	-	-	-

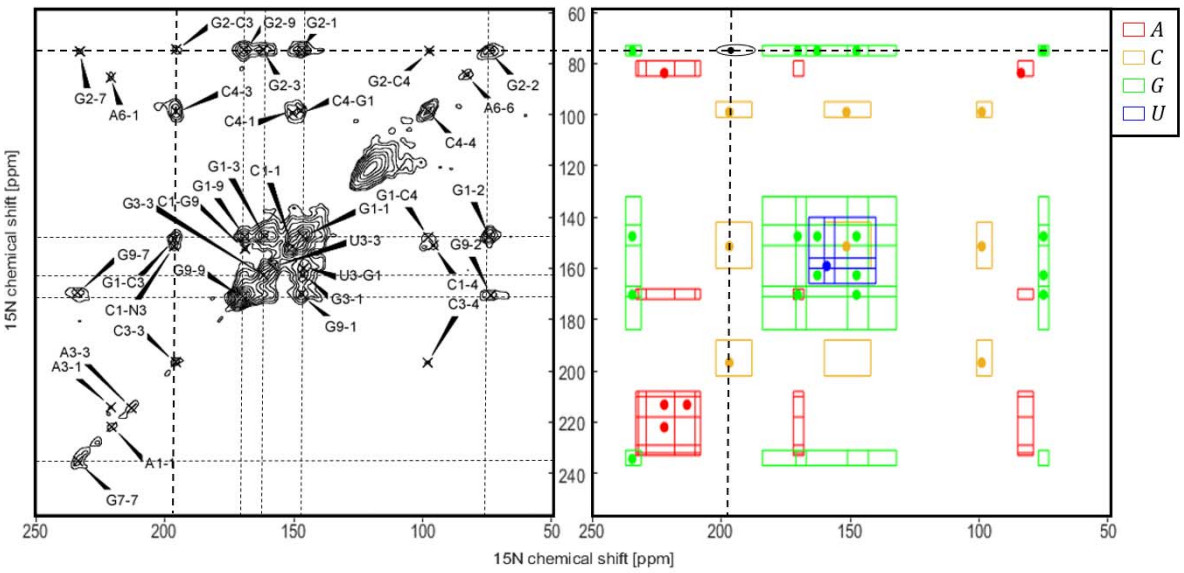

Figure 2: (a) A 2D 15N-15N typical PDSD spectrum of the MS2 RNA. A, C, G and U stand for the different nucleotides. Numbers identify the particular nitrogen in the nucleotide following BMRB nomenclature. Dashed lines mark the chemical shifts of G and intersects between lines correspond to intra-nucleotide cross-peaks. The spectrum was acquired with a mixing time of 16s at a spinning speed of 8 kHz, and a temperature set to -28°C. The spectrum was processed with an exponential line broadening of 100Hz in both dimensions. Twenty contours at multiples of 1.4 were generated with lowest contour set to a signal to noise ratio of 5. (b) A theoretical plot of the most-probable position of RNA intra-nucleotide signals. Coloured squares, different for each nucleotide, are centred around the average value of a particular peak according to BMRB with their size corresponding to the standard deviation. Points mark the position of intra-nucleotide peaks observed in our spectra. The black ellipse represents an example of a hydrogen bond between G2 and C3 (see below).

Identification of hydrogen bonds. Once ^{15}N shifts have been assigned, several inter-nucleotide contacts could be identified. Those are attributed almost exclusively to base-pairing interactions, which are characteristic of the helical double-strand-like secondary structure of the RNA (in MS2, 68% of the RNA that appears in the electron density maps is in attributed to base-pairing arrangement). In Fig. 2b, the schematics of the RNA spectrum,

the position of a representative cross-peak is given by the ellipse, correlating G2 and C3 belonging to a G-C canonical WC base-pair.

A clear evidence for base-pairing interactions is shown in the different ^{15}N-^{15}N spectra shown in figure 3. We can identify G-C base-pairing via the contacts G1-C3 and G2-C3. We can also identify C4-G3, and C4-G1. Although the PDSD experiment is not sufficiently quantitative, the fact the G1-C3 is the strongest cross-peak suggest that these contacts are typical of WC pairs. All other contacts match this type of hydrogen bond. According to a CryoEM structure by Dai et. al. (34), analysis of RNA secondary structure elements shows that ~54% of the hydrogen bonds in the structure are formed between G and C. That coincides with the fact that most hydrogen bond correlations found in our spectra were between these two nucleotides. Such a base pair involves 5 proton spins available to mediated magnetization transfer, while other contacts have less. Additionally, all spectra show higher intensities for guanine ^{15}N signals, followed by cytosine. G and C also appear more frequently in the MS2 RNA. Another canonical base pair is expected between A and U, and mainly A1/6 and U3 assuming that the WC face is the most common arrangement. However, we could not detect such contacts. Both diagonal signals of A6 and A1 are relatively weak. This is not surprising given the fact that for adenine only the proton of C2 is available to enhance the polarization generated by the N6 amine protons. We observe even weaker A1-A6 and A1-A3 cross-peaks at long mixing times. Thus, the expected cross-peaks of A1-U3 at 222.0-159.1 ppm, or A6-U3 at 83.8-159.1 are probably too weak to detect (uracil contributes only a single proton to the hydrogen bond). Given the fact that A-U base pairs are stabilized by two hydrogen-bonds (and 3 protons), while those of G-C by three hydrogen-bonds (and 5 protons), it is likely that the A-U pair is also more mobile and thus the ^{15}N-^{15}N dipolar interaction is too weak due to some motional averaging.

In addition to the G-C canonical base pair, RNA structure is also based on the formation of G-U wobble base pairs (45). Interestingly, we observe (figure 3c) clear G1-U3 correlations between these two nucleotides, corresponding to the WC edge. Despite being energetically similar to the A-U base pair, the additional proton contributed by G, and its much preferred excitation efficiency provides sufficient polarization for this hydrogen-bond to be detected. The assignment to U3 of the peak at 159.1 ppm is based on the absence of any other correlations to G, where the G3 resonance at 162.3 is strongly correlated to G2 and G9. According to the CryoEM structure, approximately 9% of the hydrogen bonds are formed between G and U.

Three additional uncommon contacts were observed in our spectra. Correlation peaks between G and A (G3-A1, G3-A3, G3-A6) could only be found in the PDSD-RFDR experiments. This kind of hydrogen bond was reported for bacterial ribosomal RNA, where A7 (part of the Hoogsteen edge) forms a bond with G1 (part of the WC edge) (46) . However, in the case of G3-A3 correlation, both atoms are part of the sugar edge of the nucleotide. Another possibility is that some weak stacking interactions are detected, that correspond to the positioning of the N3 atoms at distances smaller then 4Å in space, or even closer if they belong to a curved region. Indeed, in the MS2 PDB structure a few such contacts could be detected. A weak (SNR of 5) A6-C4 contact is also detected (figure 3a) in the PDSD-RFDR

8s spectrum. The low intensity can indicate a low abundance hydrogen bond, or more likely, a stacking interaction.

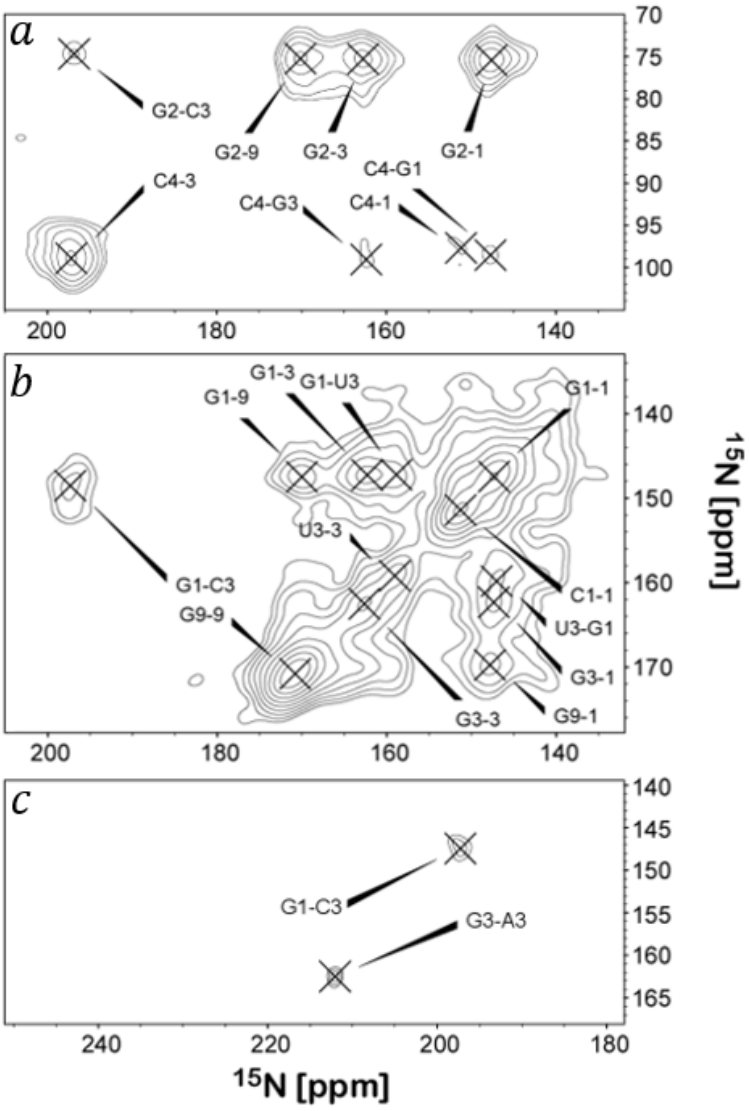

Figure 3: Examples of hydrogen bond and additional inter-nucleotide cross-peaks from different 15N-15N spectra. The contour level was set such that the lowest signal had an SNR of 5. (a) PDSD-RFDR with a mixing time of 8 sec. (b) PDSD with a mixing time of 16 sec. Only the cross-peaks corresponding to a hydrogen bond were assigned. This plots shows the G-U wobble pair. (c) PDSD-RFDR, 2 sec.

In all the spectra we examined there were no signals that we could correlate to non-base-paired nucleotides. This can be due to lack of resolution, but perhaps more likely due to lower occurrence of non-base-paired nucleotides in the structure. As all our spectra required temperatures below -25C, since at higher temperatures even the spectra reported above could not be observed, it is possible that more dynamics RNA parts are missing.

Improving polarization transfer with ^{1}H-RFDR. The homonuclear interaction between ^{13}C spins is significantly stronger than that of ^{15}N spin pairs and therefore short mixing times (10-500 ms) are sufficient for magnetization transfer. Moreover, by constantly irradiating on the ^{1}H spins at a field that resonates with the spinning frequency ($\gamma B_1=\nu_R$), known as dipolar assisted rotational resonance (47), enhanced magnetization transfer is obtained. Yet, irradiating for seconds, as required for ^{15}N recoupling, is in practice impossible due to hardware limitations and therefore using DARR for ^{15}N correlation experiment is not always feasible. Moreover, RNA is a dynamics molecule with a smaller density of proton spins as compared to proteins, further reducing the efficiency of dipolar recoupling. ^{15}N correlation spectra in biological samples are therefore mostly obtained by the PDSD technique with the application of long mixing times (48, 49) in the order of seconds, or using direct polarization transfer via the application of rotor-synchronous ^{15}N π pulses (23). At

high spinning speeds, the PAR (proton assisted recoupling) technique has been proved useful (25, 50). PDSD is based on an indirect effect, in which the ^{15}N-^{15}N magnetization transfer is achieved due to ^{1}H-^{15}N dipolar recoupling (resulting from incomplete MAS averaging of this interaction).

Long mixing time required for ^{15}N correlations always carry some signal decay due to relaxation and as the mixing times in our studies was increased from 2 to 16 sec, the SNR was reduced by up to 7-fold in some cases (see Table S2 in the SI). On the other hand, new signals appeared. Although the homonuclear ^{1}H-^{1}H dipolar interaction is theoretically not necessary for the PDSD effect to occur (51), clearly enhanced ^{1}H-^{1}H interaction can increase the efficiency of ^{1}H-^{15}N heteronuclear dipolar recoupling. We therefore applied synchronous π pulses to the ^{1}H channel following the RFDR scheme in order to directly recouple the ^{1}H-^{1}H homonuclear dipolar interaction. As demonstrated in figure S1 in SI, this approach is different from the original suggestion to recouple directly heteronuclear interaction by applying two pulses every rotor period (51), or directly recoupling the homonuclear ^{15}N dipolar interaction using synchronous π pulses(52). Four ^{15}N-^{15}N correlation experiments were conducted – two with a mixing time of 2s, and two with a mixing time of 8s, each pair differing only by the application of the ^{1}H-RFDR sequence. The overlay between the spectra is shown in figure 4. Although the average SNR at long mixing times is generally smaller, for most cross-peaks, the signal to noise ratio has consistently increased (average of ~165% for the mixing time of 2 sec, and of ~127% for 8 sec) by the application of the π pulses. Moreover, not only does the PDSD-RFDR spectrum contain more correlations, these correlations are mostly between two hydrogen-bonded nitrogen spins thus providing essential additional information regarding the hydrogen bonds patterns in the RNA, enabling detection of the data described in previous sections. The actual SNR enhancement in both experiments are given in Tables S3a and S3b of the SI.

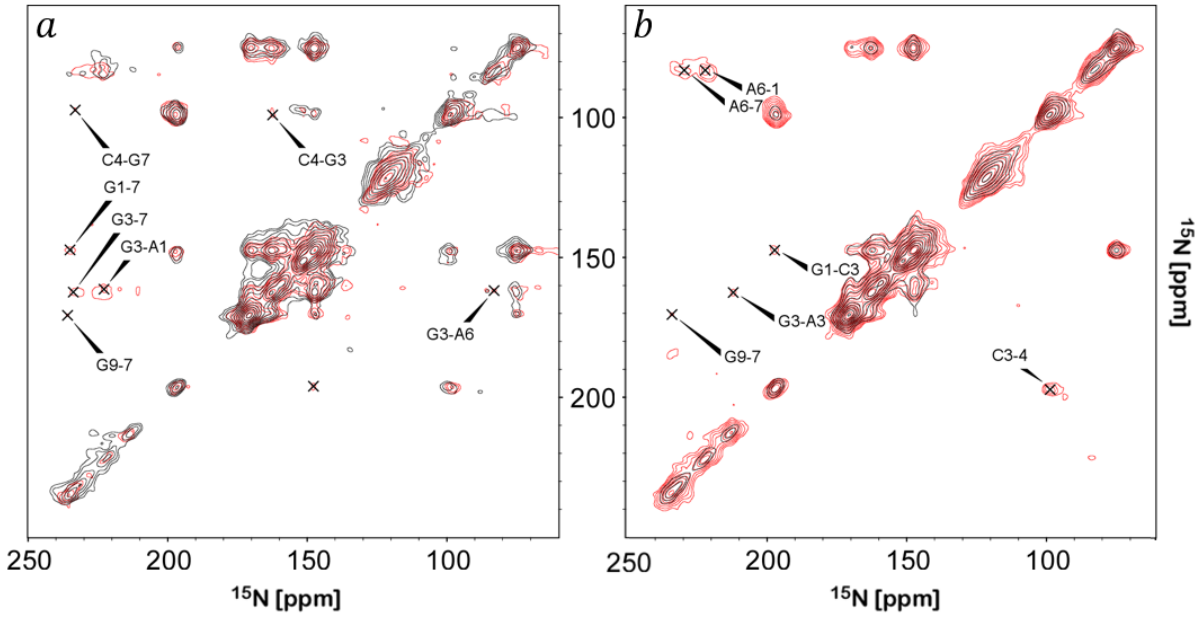

Figure 4: A comparison between PDSD (black) and PDSD-RFDR (red) ^{15}N-^{15}N correlation spectra acquired with a similar mixing time of (a) 8 sec and (b) 2 sec. Cross-peaks that appear only in the PDSD-RFDR

experiment are assigned. Enhancement is also apparent in many other signals, averaging ~126% (8s) and ~153% (2s) for the cross-peaks. The contour levels were chosen such that the lowest SNR was 5. The processing (100Hz broadening, similar zero-filling, similar acquisition times) was identical in all cases.

The enhancing effect of the π pulses can be reproduced qualitatively also using numerical simulations. Using the SIMPSON software (42), we calculated the polarization transfer between two non-hydrogen (X) spins in a X_2H_3 spin system, where all spins are coupled by hetero- and homonuclear interactions. We followed in two cases the evolution of a preliminary state in which the two X spins are oppositely polarized; one with the π pulses (PDSD-RFDR), and another without. The numerical simulations shown in Fig. S2 show that indeed polarization transfer is enhanced with the π pulses verifying our experimental results.

Summary and Conclusions

The 1.1MDa full-length RNA isolated directly from the MS2 bacteriophage virus was studied using solid state NMR techniques. Using RFDR-enhanced proton-driven-spin-diffusion ^{15}N-^{15}N correlation experiments, we could assign the ^{15}N resonances to the four different nucleotides, and detect hydrogen bonds, both canonical as well as wobble base pairs. These hydrogen bonds stabilize the secondary structure of the viral RNA and reduce its overall dynamics. By recognizing the ^{15}N shifts making up the hydrogen bonds, it is possible with such techniques to determine the face of the bond and the dominant pairs we detect have a Watson-Crick face.

While we show how solid-state NMR can be useful to study such high-molecular-weight RNA, detection of genomic ^{15}N resonances in general, and more importantly hydrogen bonds, poses some challenges, some of which we have addressed here. Excitation of ^{15}N signals is based on polarization transfer from ^{1}H, and is therefore less efficient for tertiary amines and in particular in nucleotides bearing less proton spins. Thus guanine and cytosine signals dominate the spectral features. Another challenge is the ability to transfer polarization between ^{15}N nuclei, which relies on the interaction with protons. While the standard techniques (at average spinning speeds) require extension of mixing times, the cost is signal decay due to T_1 relaxation. Moreover, this increases significantly the total experimental time. We show here that by recoupling the ^{1}H-^{1}H dipolar interaction using radio-frequency driven-recoupling, signal enhancement is obtained without a need for seconds-long continuous irradiation that challenges the hardware. Consequently, the experimental time can be shortened significantly. It also allows gaining information even when long mixing times are inapplicable due to shorter relaxation times. Moreover, using this technique we have been able to detect new correlations not detected even at very long mixing times. Some of these correlations validate our assignment. Others are attributed to inter-nucleotide contacts. Towards more quantitative estimation of hydrogen bond patterns, it will be required to generate a more uniform and efficient ^{15}N excitation, and estimate and fit polarization transfer between base pairs (53). The latter is required even if such hydrogen bonds are detected directly via proton detection (25).

The improved method we described how solid-state for characterizing hydrogen bonds in intact RNA using solid-state NMR is applicable to RNA molecules extracted from natural sources and can be utilized regardless of sequence length. Although not yet quantitative, it can potentially guide structure prediction by serving as structure restraints.

Acknowledgments

This research was supported by the Israel Science Foundation grant #847/17. We thank Prof. Uri Gophna from Faculty of Life Sciences, Tel Aviv University, for supplying MS2 stocks, and for fruitful discussions.

References

1. Eddy,S.R. (2001) Non–coding RNA genes and the modern RNA world. *Nat. Rev. Genet.*, **2**, 919–929.
2. Ransohoff,J.D., Wei,Y. and Khavari,P.A. (2018) The functions and unique features of long intergenic non-coding RNA. *Nat. Rev. Mol. Cell Biol.*, **19**, 143–157.
3. Flynn,R.A., Pedram,K., Malaker,S.A., Batista,P.J., Smith,B.A.H., Johnson,A.G., George,B.M., Majzoub,K., Villalta,P.W., Carette,J.E., *et al.* (2021) Small RNAs are modified with N-glycans and displayed on the surface of living cells. *Cell*, 10.1016/j.cell.2021.04.023.
4. Park,C.-J. (2003) Solution structure of the influenza A virus cRNA promoter: implications for differential recognition of viral promoter structures by RNA-dependent RNA polymerase. *Nucleic Acids Res.*, **31**, 2824–2832.
5. Barnwal,R.P., Yang,F. and Varani,G. (2017) Applications of NMR to structure determination of RNAs large and small. *Arch. Biochem. Biophys.*, **628**, 42–56.
6. Westhof,E. (2015) Twenty years of RNA crystallography. *RNA*, **21**, 486–487.
7. Sugita,Y., Matsunami,H., Kawaoka,Y., Noda,T. and Wolf,M. (2018) Cryo-EM structure of the Ebola virus nucleoprotein–RNA complex at 3.6 Å resolution. *Nature*, **563**, 137–140.
8. Ennifar,E., Nikulin,A., Tishchenko,S., Serganov,A., Nevskaya,N., Garber,M., Ehresmann,B., Ehresmann,C., Nikonov,S. and Dumas,P. (2000) The crystal structure of UUCG tetraloop 1 1Edited by J Doudna. *J. Mol. Biol.*, **304**, 35–42.
9. Wang,Z., Hartman,E., Roy,K., Chanfreau,G. and Feigon,J. (2011) Structure of a Yeast RNase III dsRBD Complex with a Noncanonical RNA Substrate Provides New Insights into Binding Specificity of dsRBDs. *Structure*, **19**, 999–1010.
10. Ahmed,M., Marchanka,A. and Carlomagno,T. (2020) Structure of a Protein–RNA Complex by Solid□State NMR Spectroscopy. *Angew. Chemie*, **132**, 6933–6940.
11. Marchanka,A., Simon,B., Althoff-Ospelt,G. and Carlomagno,T. (2015) RNA structure determination by solid-state NMR spectroscopy. *Nat. Commun.*, **6**, 7024.
12. Duss,O., Maris,C., von Schroetter,C. and Allain,F.H.-T. (2010) A fast, efficient and sequence-independent method for flexible multiple segmental isotope labeling of RNA using ribozyme and RNase H cleavage. *Nucleic Acids Res.*, **38**, e188–e188.
13. Marchanka,A., Kreutz,C. and Carlomagno,T. (2018) Isotope labeling for studying RNA by solid-state NMR spectroscopy. *J. Biomol. NMR*, **71**, 151–164.
14. Turner,D.H., Sugimoto,N. and Freier,S.M. (1988) RNA Structure Prediction. *Annu. Rev. Biophys. Biophys. Chem.*, **17**, 167–192.
15. Reuter,J.S. and Mathews,D.H. (2010) RNAstructure: software for RNA secondary structure prediction and analysis. *BMC Bioinformatics*, **11**, 129.

16. Strobel,E.J., Yu,A.M. and Lucks,J.B. (2018) High-throughput determination of RNA structures. *Nat. Rev. Genet.*, **19**, 615–634.
17. LEONTIS,N.B. and WESTHOF,E. (2001) Geometric nomenclature and classification of RNA base pairs. *RNA*, **7**, S1355838201002515.
18. Ladizhansky,V. (2017) Applications of solid-state NMR to membrane proteins. *Biochim. Biophys. Acta - Proteins Proteomics*, **1865**, 1577–1586.
19. Lecoq,L., Fogeron,M.-L., Meier,B.H., Nassal,M. and Böckmann,A. (2020) Solid-State NMR for Studying the Structure and Dynamics of Viral Assemblies. *Viruses*, **12**, 1069.
20. Habenstein,B. and Loquet,A. (2016) Solid-state NMR: An emerging technique in structural biology of self-assemblies. *Biophys. Chem.*, **210**, 14–26.
21. Sreemantula,A.K. and Marchanka,A. (2020) Solid-state NMR spectroscopy for characterization of RNA and RNP complexes. *Biochem. Soc. Trans.*, **48**, 1077–1087.
22. Yang,Y. and Wang,S. (2018) RNA Characterization by Solid-State NMR Spectroscopy. *Chem. - A Eur. J.*, **24**, 8698–8707.
23. Leppert,J. (2004) Identification of NH...N hydrogen bonds by magic angle spinning solid state NMR in a double-stranded RNA associated with myotonic dystrophy. *Nucleic Acids Res.*, **32**, 1177–1183.
24. Riedel,K., Leppert,J., Ohlenschla,O. and Go,M. (2005) Characterisation of hydrogen bonding networks in RNAs via magic angle spinning solid state NMR spectroscopy. *J. Biomol. NMR*, **31**, 331–336.
25. Yang,Y., Xiang,S., Liu,X., Pei,X., Wu,P., Gong,Q., Li,N., Baldus,M. and Wang,S. (2017) Proton-detected solid-state NMR detects the inter-nucleotide correlations and architecture of dimeric RNA in microcrystals. *Chem. Commun.*, **53**, 12886–12889.
26. Callanan,J., Stockdale,S.R., Shkoporov,A., Draper,L.A., Ross,R.P. and Hill,C. (2020) Expansion of known ssRNA phage genomes: From tens to over a thousand. *Sci. Adv.*, **6**, eaay5981.
27. Wu,F., Zhao,S., Yu,B., Chen,Y.-M., Wang,W., Song,Z.-G., Hu,Y., Tao,Z.-W., Tian,J.-H., Pei,Y.-Y., *et al.* (2020) A new coronavirus associated with human respiratory disease in China. *Nature*, **579**, 265–269.
28. Carrasco-Hernandez,R., Jácome,R., López Vidal,Y. and Ponce de León,S. (2017) Are RNA Viruses Candidate Agents for the Next Global Pandemic? A Review. *ILAR J.*, **58**, 343–358.
29. Fiers,W., Contreras,R., Duerinck,F., Haegeman,G., Iserentant,D., Merregaert,J., Min Jou,W., Molemans,F., Raeymaekers,A., Van den Berghe,A., *et al.* (1976) Complete nucleotide sequence of bacteriophage MS2 RNA: primary and secondary structure of the replicase gene. *Nature*, **260**, 500–507.
30. Sugiyama,T., Hebert,R.R. and Hartman,K.A. (1967) Ribonucleoprotein complexes formed between bacteriophage MS2 RNA and MS2 Protein in vitro. *J. Mol. Biol.*, **25**, 455–463.
31. Valegård,K., Murray,J.B., Stonehouse,N.J., van den Worm,S., Stockley,P.G. and Liljas,L. (1997) The three-dimensional structures of two complexes between recombinant MS2 capsids and RNA operator fragments reveal sequence-specific protein-RNA interactions. *J. Mol. Biol.*, **270**, 724–738.
32. Helgstrand,C. (2002) Investigating the structural basis of purine specificity in the structures of MS2 coat protein RNA translational operator hairpins. *Nucleic Acids Res.*, **30**, 2678–2685.
33. Koning,R.I., Gomez-Blanco,J., Akopjana,I., Vargas,J., Kazaks,A., Tars,K., Carazo,J.M. and Koster,A.J. (2016) Asymmetric cryo-EM reconstruction of phage MS2 reveals genome structure in situ. *Nat. Commun.*, **7**, 12524.

34. Dai,X., Li,Z., Lai,M., Shu,S., Du,Y., Zhou,Z.H. and Sun,R. (2017) In situ structures of the genome and genome-delivery apparatus in a single-stranded RNA virus. *Nature*, **541**, 112–116.
35. Szeverenyi,N.M., Sullivan,M.J. and Maciel,G.E. (1982) Observation of spin exchange by two-dimensional fourier transform 13C cross polarization-magic-angle spinning. *J. Magn. Reson.*, **47**, 462–475.
36. Bennett,A.E., Griffin,R.G., Ok,J.H. and Vega,S. (1992) Chemical shift correlation spectroscopy in rotating solids: Radio frequency□driven dipolar recoupling and longitudinal exchange. *J. Chem. Phys.*, **96**, 8624–8627.
37. Morag,O., Sgourakis,N.G., Abramov,G. and Goldbourt,A. (2018) Filamentous Bacteriophage Viruses: Preparation, Magic-Angle Spinning Solid-State NMR Experiments, and Structure Determination. In.pp. 67–97.
38. Meir,M., Harel,N., Miller,D., Gelbart,M., Eldar,A., Gophna,U. and Stern,A. (2020) Competition between social cheater viruses is driven by mechanistically different cheating strategies. *Sci. Adv.*, **6**, eabb7990.
39. Bertani,P., Raya,J. and Bechinger,B. (2014) 15N chemical shift referencing in solid state NMR. *Solid State Nucl. Magn. Reson.*, **61–62**, 15–18.
40. Delaglio,F., Grzesiek,S., Vuister,G., Zhu,G., Pfeifer,J. and Bax,A. (1995) NMRPipe: A multidimensional spectral processing system based on UNIX pipes. *J. Biomol. NMR*, **6**.
41. Lee,W., Tonelli,M. and Markley,J.L. (2015) NMRFAM-SPARKY: enhanced software for biomolecular NMR spectroscopy. *Bioinformatics*, **31**, 1325–1327.
42. Bak,M., Rasmussen,J.T. and Nielsen,N.C. (2000) SIMPSON: A General Simulation Program for Solid-State NMR Spectroscopy. *J. Magn. Reson.*, **147**, 296–330.
43. Abramov,G. and Goldbourt,A. (2014) Nucleotide-type chemical shift assignment of the encapsulated 40 kbp dsDNA in intact bacteriophage T7 by MAS solid-state NMR. *J. Biomol. NMR*, **59**, 219–230.
44. Higman,V.A. (2018) Solid-state MAS NMR resonance assignment methods for proteins. *Prog. Nucl. Magn. Reson. Spectrosc.*, **106–107**, 37–65.
45. Varani,G. and McClain,W.H. (2000) The G·U wobble base pair. *EMBO Rep.*, **1**, 18–23.
46. Traub,W. and Sussman,J.L. (1982) Adenine-guanine base pairing in ribosomal RNA. *Nucleic Acids Res.*, **10**, 2701–2708.
47. Takegoshi,K., Nakamura,S. and Terao,T. (2001) – dipolar-assisted rotational resonance in magic-angle spinning NMR. *Chem. Phys. Lett.*, **344**, 631–637.
48. Giraud,N., Blackledge,M., Böckmann,A. and Emsley,L. (2007) The influence of nitrogen-15 proton-driven spin diffusion on the measurement of nitrogen-15 longitudinal relaxation times. *J. Magn. Reson.*, **184**, 51–61.
49. Traaseth,N.J., Gopinath,T. and Veglia,G. (2010) On the Performance of Spin Diffusion NMR Techniques in Oriented Solids: Prospects for Resonance Assignments and Distance Measurements from Separated Local Field Experiments. *J. Phys. Chem. B*, **114**, 13872–13880.
50. Lewandowski,J.R., Paëpe,G. De, Eddy,M.T. and Griffin,R.G. (2009) 15 N− 15 N Proton Assisted Recoupling in Magic Angle Spinning NMR. *J. Am. Chem. Soc.*, **131**, 5769–5776.
51. Takegoshi,K., Nakamura,S. and Terao,T. (2003) 13C–1H dipolar-driven 13C–13C recoupling without 13C rf irradiation in nuclear magnetic resonance of rotating solids. *J. Chem. Phys.*, **118**, 2325–2341.
52. Robyr,P., Meier,B.H. and Ernst,R.R. (1989) Radio-frequency-driven nuclear spin diffusion in solids. *Chem. Phys. Lett.*, **162**, 417–423.
53. Duong,N.T., Raran-Kurussi,S., Nishiyama,Y. and Agarwal,V. (2020) Can proton-proton

recoupling in fully protonated solids provide quantitative, selective and efficient polarization transfer? *J. Magn. Reson.*, **317**, 106777.

54. Sambrook,J. and Russel,D.W. (2001) Molecular Cloning: A Laboratory Manual.